Unraveling the temperature and voltage dependence of magnetic field effects in organic semiconductors

Unraveling the temperature and voltage dependence of magnetic field effects in organic semiconductors

Paul Janssen, Steinar H. W. Wouters, Matthijs Cox, and Bert Koopmans

Citation: Journal of Applied Physics **114**, 174909 (2013); doi: 10.1063/1.4827864
View online: http://dx.doi.org/10.1063/1.4827864
View Table of Contents: http://scitation.aip.org/content/aip/journal/jap/114/17?ver=pdfcov
Published by the AIP Publishing

Unraveling the temperature and voltage dependence of magnetic field effects in organic semiconductors

Paul Janssen,[a] Steinar H. W. Wouters, Matthijs Cox, and Bert Koopmans
Department of Applied Physics, Center for NanoMaterials (cNM), Eindhoven University of Technology, PO Box 513, 5600 MB Eindhoven, The Netherlands

(Received 3 July 2013; accepted 15 October 2013; published online 6 November 2013)

In recent years, it was discovered that the current through an organic semiconductor, sandwiched between two non-magnetic electrodes, can be changed significantly by applying a small magnetic field. This surprisingly large magnetoresistance effect, often dubbed as organic magnetoresistance (OMAR), has puzzled the young field of organic spintronics during the last decade. Here, we present a detailed study on the voltage and temperature dependence of OMAR, aiming to unravel the lineshapes of the magnetic field effects and thereby gain a deeper fundamental understanding of the underlying microscopic mechanism. Using a full quantitative analysis of the lineshapes, we are able to extract all linewidth parameters and the voltage and temperature dependencies are explained with a recently proposed trion mechanism. Moreover, explicit microscopic simulations show a qualitative agreement to the experimental results. © *2013 AIP Publishing LLC*. [http://dx.doi.org/10.1063/1.4827864]

I. INTRODUCTION

One of the exciting developments in the field of organic electronics is the discovery of a surprisingly large, room temperature, magnetoresistance effect in organic semiconductor devices without any ferromagnetic components, an effect often referred to as organic magnetoresistance (OMAR).[1,2] The current through such a device, where the organic layer is sandwiched between two non-magnetic electrodes, can be changed significantly (up to 25%) by applying a small (∼mT) magnetic field. The effect can be tuned by changing the operating conditions, such as voltage, temperature, and angle between the current and magnetic field.[3–15] Recently, cheap plastic sensor technology has been proposed as an example of its application potential.[16] Nevertheless, a fundamental understanding of the interactions of spins and charges in organic semiconductors currently remains the goal of extensive experimental[1–15] and theoretical[17–19] research.

To explain OMAR, all contemporary models incorporate pairs of spin-carrying particles undergoing spin-dependent reactions. The outcome of these reactions is influenced by the intrinsic mixing of the pair's spin state and subsequent suppression thereof in an external applied magnetic field. The models then diverge on the matter of which particle reaction is at the origin of OMAR. One can mainly distinguish between the reactions of: (i) equally charged polarons into bipolarons,[19] (ii) polaronic electrons and holes,[17] and (iii) triplet excitons with polarons or other triplets.[18] Very recently, we have shown that the dominant mechanism for OMAR depends on the exact material choice and operating conditions of the device.[20] Therefore, a thorough investigation of all relevant operating conditions is crucial in understanding magnetic field effects (MFEs) in organic semiconductors.

As introduced in the foregoing, mixing of spin states plays a crucial role in OMAR, regardless of the exact underlying model. There is a growing consensus about the importance of hyperfine fields, originating from the hydrogen nuclei in the organic material, for spin mixing.[13] In this case, the lineshape of the OMAR curve is related to the hyperfine field strength, which is on the order of a millitesla and we will refer to this as a low-field effect (LFE). The lineshape is, however, not only determined by the magnitude of the hyperfine fields. From the bipolaron model, for example, it is known that even with the same hyperfine fields, additional broadening occurs when the bipolaron formation rate is increased.[19,21] Moreover, it has recently been shown that the LFE can be accompanied by a distinct magnetic field effect at ultra-small field scales (USFE, typically ≤mT).[13] Beside low-field effects, OMAR curves can also show distinct features at higher magnetic field scales (HFE, ∼20 mT up to a few Tesla). Accurately measuring and understanding the exact lineshapes of the LFE and HFE is therefore of major importance since the lineshapes can be correlated to the dominant underlying mechanism.[20]

In this chapter, we present a detailed study on the voltage and temperature dependence of OMAR, aiming to unravel the magnetic field effects on the current in pristine conjugated polymer devices. Even though OMAR has been studied extensively, there are only a few detailed reports on its temperature dependence.[2–7] Moreover, these studies mainly focus on the magnitude of the OMAR effect. We show a full quantitative analysis of the lineshape and also extract the linewidth parameters. It was demonstrated before that in organic light emitting diode (OLED) type devices, the MFEs are dominated by the reactions between (trapped) triplets and polarons.[18,22,23] A schematic overview of this mechanism is shown in Fig. 1. Here, the relevant particles and their (spin-dependent) reactions are depicted as a function of energy. We can distinguish between the rates of dissociation and recombination of singlet and triplet electron–hole pairs ($q_{S,T}$ and $k_{S,T}$) or doublet and quartet triplet–polaron pairs ($r_{D,Q}$ and $k_{D,Q}$), respectively.[23] The low magnetic field effect

[a]Electronic mail: p.janssen@tue.nl

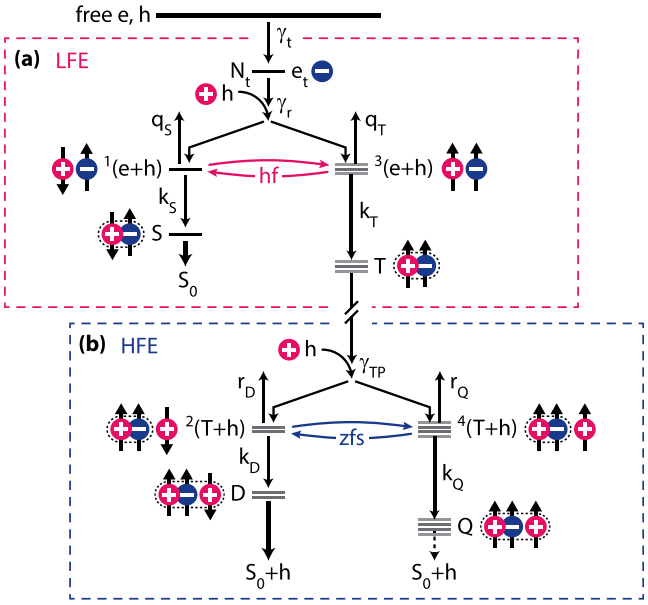

FIG. 1. A schematic overview of all relevant particles and reactions of the trion model. (a) The low magnetic field effect (LFE) originates from mixing of polaronic electron–hole pairs by hyperfine fields (hf). (b) Whereas the mixing of triplet exciton–polaron pairs at the zero field ZFS leads to a high-field effect (HFE).

(LFE) originates from mixing of precursor pairs by hyperfine fields (hf); whereas the mixing of triplet exciton–polaron pairs at the zero field splitting field scale (ZFS) leads to a high-field effect (HFE). By studying the MFE lineshapes as a function of voltage and temperature, we obtain a deeper understanding of these triplet–polaron reactions.

II. METHODS

A. Device fabrication

In this work, we studied the magnetic field effects on the current for devices consisting of a phenyl substituted poly(1,4-phenylenevinylene) semiconducting polymer called Super Yellow PPV (SY-PPV, Merck, used as received). The SY-PPV is dissolved in orthodichlorobenzene (ODCB) at a concentration of 8 mg/ml, and stirred on a hot plate at 50 °C for at least 2 h. The devices were prepared on glass substrates with patterned indium tin oxide (ITO) anodes. After careful cleaning, followed by a UV-ozone treatment, a thin layer of poly(3,4/ethylenedioxythipophene):poly(styrenesulfonate) (PEDOT:PSS) was applied by spin coating. The SY-PPV was spin coated at 1200 RPM for 60 s, resulting in a layer thickness of 100 nm. Subsequently, the samples were transferred to a nitrogen filled glove box where the cathode, consisting of LiF and Al, was evaporated in a high vacuum system ($\leq 10^7$ mbar). From this point on, the samples always remained in a dry nitrogen environment. The total junction stack thus consists of ITO/PEDOT:PSS(60 nm)/SY-PPV (100 nm)/LiF(1 nm)/Al(100 nm).

B. Measurements

Magnetic field effect measurements were performed in a cryostat that is attached to a glovebox with a dry nitrogen environment ($[O_2] < 0.3$ ppm, $[H_2O] < 0.3$ ppm) and the sample temperature can be controlled from 10 K up to room temperature. The cryostat is placed between the poles of an electromagnet, which allows us to apply an external magnetic field up to 0.5 T, with an accuracy of 50 μT. The devices were driven at a constant voltage V using a Keithley 2400 Series SourceMeter. We measured the current I through the device while sweeping the magnetic field B. From this measurement, the magnetoconductance (MC) was calculated with $\mathrm{MC}(B) = [I(B) - I(0)]/I(0)$.

C. Empirical lineshapes

In this study, we analyzed the magnetoconductance as a function of magnetic field MC(B) for different voltages and temperatures (refer to Fig. 2 for a typical result). To analyze the experimental results, we used the following fitting function:

$$\mathrm{MC}(B) = \mathrm{LFE} \cdot f(B, B_{\mathrm{hf}}, B_{\mathrm{m}}, r) + \mathrm{HFE} \cdot \frac{B^2}{(|B| + B_{\mathrm{HFE}})^2}. \quad (1)$$

The function $f(B, B_{\mathrm{hf}}, B_{\mathrm{m}}, r)$, with $f\ (B=0)=0$ and $f(B=\infty)=1$, is explained in full detail in Ref. 21. The function correctly describes the LFE including the ultra-small-field effect, as is shown in the left panel of Fig. 2(a)

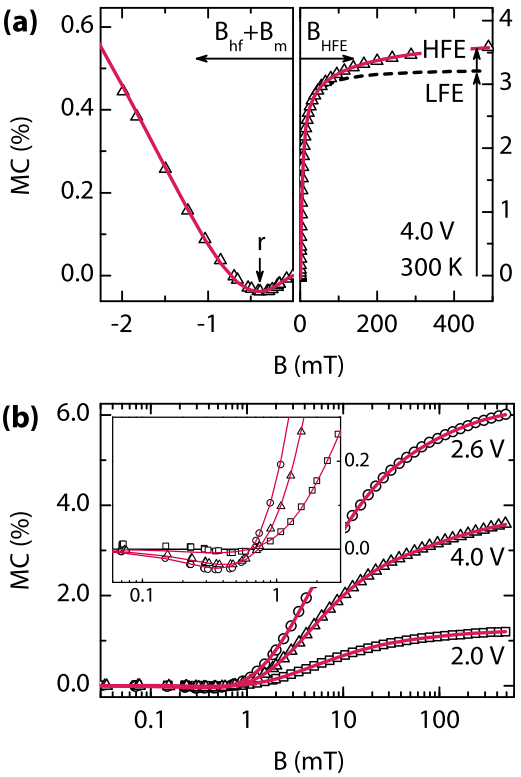

FIG. 2. Magnetoconductance as a function of magnetic field. (a) Experimental result for a bias voltage of 4.0 V at room temperature. The solid line is a fit using the empirical lineshape Eq. (1), where the low (LFE) and high magnetic field (HFE) contributions are separately depicted. The magnitude of LFE and HFE and their corresponding linewidth parameters (B_{hf}, B_{m}, r, and B_{HFE}) are also shown. (b) Magnetoconductance as a function of magnetic field on a logarithmic scale for different bias voltages. The inset shows a close-up of the USFE.

and the inset of Fig. 2(b). This empirical function allows us to separately extract the role of the intrinsic hyperfine field (B_{hf}) and the extrinsic additional broadening (B_m) induced by the microscopic mechanism. The function converges to a Lorentzian lineshape for $f(B_m = 0)$ and a so-called non-Lorentzian for $f(B_m \gg 0)$. The USFE is incorporated by the parameter r, which describes the limit in which hopping of carriers is no longer slow compared to spin precession in the hyperfine fields. The high-field effect (HFE) is fitted with non-Lorentzian lineshape and has a characteristic linewidth B_{HFE}. In the fitting procedure, the hyperfine field B_{hf} is a shared fitting parameter, whereas the other parameters (LFE, B_m, r, HFE, and B_{HFE}) can vary with temperature and voltage.

III. RESULTS AND DISCUSSION

A. Current density

In order to fully understand the voltage and temperature dependence of the magnetic field effects, we first need to address the effects on the current without an applied magnetic field. Therefore, we have measured the current density J as a function of voltage V for different temperatures T and the results are shown in Fig. 3. We can identify three transport regimes: (i) an ohmic leakage current at the lowest voltages, (ii) a diffusion current in the diode regime below the built-in voltage ($V_{bi} \approx 2\,V$), with a rectifying exponential dependence $J \sim \exp(qV/nk_BT)$, and (iii) a space-charge limited current above the built-in voltage, with a power law dependence $J \sim (V - V_{bi})^n$. Using this relation, we can extract V_{bi} and n, as depicted by the solid line in Fig. 3. We obtain a power factor $n = 3.1$, whereas $n = 2$ for a trap free device with ohmic electrodes, indicating the presence of traps in the organic layer.[24]

B. Magnetic field effects

To investigate the magnetic field effect on the current, we have systematically measured the magnetoconductance as a function of magnetic field, bias voltage, and temperature. We have analyzed the results by fitting this extensive experimental data set using Eq. (1), which allows us to unravel the lineshape of the MFE as a function of voltage and temperature. A typical result is shown in Fig. 2. It is found that the lineshapes are accurately described, thereby obtaining reliable values for the amplitudes and linewidth parameters of the low- and high-field effects. Moreover, the ultra-small-field effect is also accurately characterized. We will start our discussion with the amplitudes of the MFEs. Thereafter, we will address the linewidths.

The magnitude of the low- and high-field effects as a function of voltage and temperature is shown in Figs. 4(a) and 4(b), respectively. Both magnetic field effects show a very characteristic MC(V) dependence, vanishing below the built-in voltage and peaking somewhat above. Both the onset as well as the peak value of the MFEs shift to higher voltages with decreasing temperature. Finally, it was shown that the magnetic field effect on the current in pristine organic semiconductors is predominantly governed by the reactions between triplet excitons and polarons.[18,20,22,23,25] Moreover, Cox *et al.* recently proposed an analytical model where these reactions are described by the spin-selective formation of so-called metastable trions from triplet exciton–polaron pairs.[23] Their model provides an intuitive explanation of the MC(V) dependence. The initial increase originates from the increase of triplet density with voltage, while the eventual decrease can be assigned to a saturation of trap filling.

In addition to this qualitative explanation, we analyzed the MC(V)-curves using the analytical model as proposed by Cox *et al.* To describe the amplitude of the low-field effect, only two free fitting parameters are used: the onset voltage V_{on} and the triplet–polaron interaction coefficient γ_{TP}. The other parameters such as the trap density ($N_t \sim 10^{-4}\,nm^3$), electron trap coefficient ($\gamma_t \sim 10^5\,nm^3s^{-1}$), electron–hole

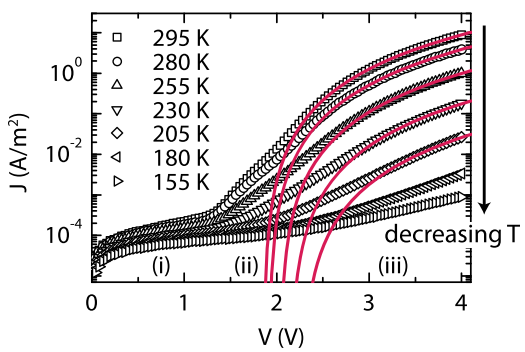

FIG. 3. Current density as a function of voltage for different temperatures. Three regimes are depicted: (i) an ohmic leakage current, (ii) a diffusion current below the built-in voltage ($V_{bi} \approx 2\,V$), and (iii) a space-charge limited current above the built-in voltage. The solid line is a power law fit for the space-charge limited regime.

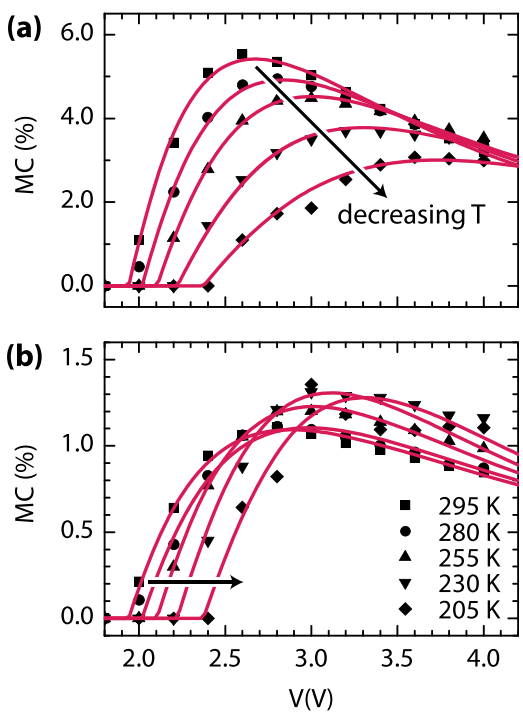

FIG. 4. Magnetic field effects as a function of voltage for different temperatures. (a) Magnitude of the LFE as a function of voltage for different temperatures. (b) Magnitude of the high-field effect (HFE) as a function of voltage for different temperatures. The solid lines are a fit using the trion model.

capture coefficient ($\gamma_R \sim 10^8\,\mathrm{nm^3 s^{-1}}$), triplet rate ($k_T \sim 10^4\,\mathrm{s^{-1}}$), and trion rate ($k_Q \sim 10^3\,\mathrm{s^{-1}}$), indicated in Fig. 1, are taken from the literature.[26–28] The resulting fits are depicted by the solid lines in Fig. 4(a) and describe the MC(V)-curves remarkably well.

To confirm the physical validity of the fitting parameters, we have plotted the onset voltage V_{on} obtained from the fit of the MC(V)-curves as a function of the built-in voltage V_{bi} as acquired from the $J(V)$-curves. The result is shown in Fig. 5(a). We observe a clear correlation between the two voltages, i.e., once the condition for bipolar charge injection is met ($V > V_{bi}$), we can measure a MFE ($V > V_{on}$), indicating the importance of both charge carriers for the measured MFE. The increase in built-in voltage with decreasing temperature is in agreement with literature results.[29,30] Furthermore, we can evaluate the triplet–polaron interaction coefficient γ_{TP} as a function of temperature. The triplet–polaron interaction has been shown to scale with temperature as $\gamma_{TP} \propto \mu_h \langle R \rangle kT$,[26] where $\langle R \rangle$ is the interaction radius. The hole mobility scales with $\mu_h \propto \exp(-\Delta/kT)$, where Δ is the activation energy.[24] The triplet–polaron interaction coefficient as a function of temperature can be described using this relation, as shown in Fig. 5(b). We find an interaction radius $\langle R \rangle \sim 10^{-9}$ m when using an activation energy $\Delta = 0.48$ eV, which is in agreement with literature values.[24]

The analytical model can also explicitly describe the magnitude of the high-field effect, as is shown in Fig. 4(b). The temperature dependence of the high-field effects is less pronounced than the low-field effect. In passing, we note that, assuming V_{on} is equal for the LFE and HFE, there is only one remaining free fitting parameter, namely the trion dissociation rate. Although the resulting fit is not as accurate as the low-field effect, it still captures the essential trends.

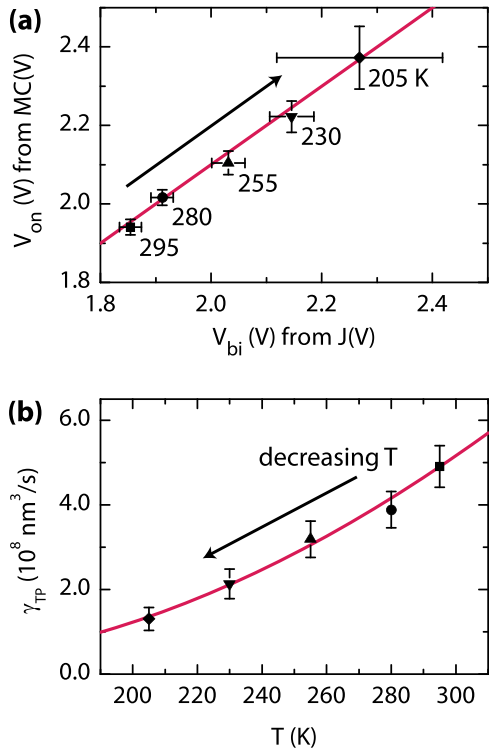

FIG. 5. Extracted model parameters as a function of temperature. (a) The onset voltage V_{on} obtained from the fit of the MC(V)-curves using the trion model compared to the built-in voltage V_{bi} as acquired from the $J(V)$-curves. The solid line is a guide to the eye showing a clear correlation between the two voltages. (b) The reaction rate between trions and free polarons γ_{TP}, extracted from the LFE, as a function of temperature.

C. Linewidth analysis

After this satisfactory description of the magnitudes of the magnetic field effects, we continue our discussion with the linewidths of the effects, where we first address the low-field effect. Figures 6(a)–6(c) show the intrinsic hyperfine field strength B_{hf}, the additional broadening of the low-field linewidth B_m, and the ratio between hopping and precession r, respectively. Using our fitting procedure, we find, as expected, no temperature dependence in the hyperfine field strength and obtain an almost identical hyperfine field strength of approximately 0.9 mT for all measurements. However, B_m and r do show a remarkable voltage and temperature dependence. In previous studies, the explicit linewidths have often been neglected. Nevertheless, studying the voltage and temperature dependency of the linewidths provides new insights in the underlying mechanisms for the MFEs on the current. The lines in Fig. 6(b) indicate a decrease in B_m with increasing voltage and temperature. To explain this dependency, we need to elucidate the exact role of the extrinsic low-field linewidth parameter. Therefore, we

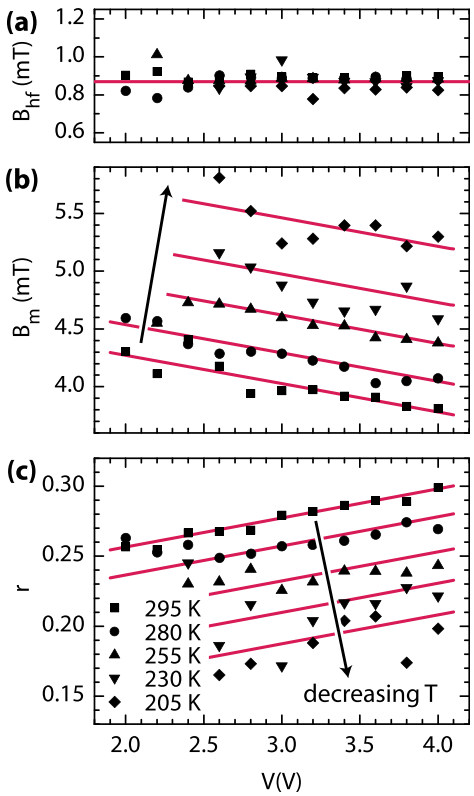

FIG. 6. Extracted low-field effect parameters as a function of voltage for different temperatures. (a) The hyperfine field strength B_{hf} showing no temperature dependence. (b) The extrinsic low-field linewidth B_m as a function of voltage and temperature. The solid lines are a guide to the eye showing a decrease in linewidth with increasing voltage and temperature. (c) The hopping ratio r as a function of voltage and temperature. The lines are a guide to the eye showing an increase in hopping rate with increasing voltage and temperature.

performed numerous simulations and investigated the linewidths of the MFEs.[21,31] The simulations reveal that additional broadening can be observed when the formation, dissociation, and recombination rates of the interacting polaron pairs are altered. Although a full description goes beyond the scope of this present chapter, a brief discussion of our findings is presented in Sec. III D.

The final parameter, which we introduced to correctly describe the ultra-small-field effect, is the ratio between hopping and precession r. Figure 6(c) shows this ratio as a function of voltage and temperature and an increase in hopping rate with increasing voltage and temperature is observed. This trend can intuitively be explained by the increase in hopping rates upon raising the bias voltage or temperature, whereas the precession frequency remains unaffected. One might naively expect a much larger dependency of r on the voltage and temperature. We conjecture that this weak dependency is caused by a distribution of hopping times.[32] Only a certain range of hopping rates contribute to the MFEs in the current, because the fastest hops are not influenced by hyperfine based mixing mechanisms and the slowest hops hardly contribute to the total current. Changing the voltage or temperature only shifts the small range of hops which contribute to the MFEs.

Finally, we will discuss the linewidth of the high-field effect. The width of the HFE, caused by triplet–polaron interactions, is known to be related to the zero-field splitting (B_{ZFS}) of the triplet excitons, which is independent of temperature. Yet, in contrast to the hyperfine field strength, the linewidth of the high-field effect does show a clear voltage and temperature dependence, as can be seen in Fig. 7. We attribute this difference to our description of the high-field effect, which is characterized by a single linewidth parameter B_{HFE}. We propose that the high-field effect also has an intrinsic component, governed by the zero-field splitting rather than the hyperfine field, and an additional broadening parameter. This additional broadening will also be briefly discussed using simulations in Sec. III D.

D. Simulations

In all the models that have been proposed for OMAR, the magnetic-field dependent reactions of the spin carrying particles play an essential role. Schellekens *et al.* used an adapted Stochastic Liouville equation in a density-matrix formalism to successfully perform calculations on magnetic field effects in organic semiconductors.[31] We have used their approach to simulate magnetic field effects caused by triplet–polaron interactions. The calculations for the LFE and HFE, indicated by the dashed boxes in Fig. 1, are schematically depicted in Figs. 8(a) and 9(a), respectively. We calculated the influence of changes in the different recombination and dissociation rates on the MFEs lineshapes.

For the LFE, the simulations reveal that additional broadening can be observed when the recombination and dissociation rates for singlets (k_S, q_S) and triplets (k_T, q_T) are varied, as is clearly shown in Fig. 8(b). We have analyzed the LFE lineshape using Eq. (1), where we have fixed the value of the hyperfine field strength so that the only free fitting parameter is the extrinsic broadening parameter B_m. The results are shown in Fig. 8(c). Increasing the dissociation rate, while keeping the other rates in the system constant, causes less broadening of the MC(B)-curves, as described by a decrease in B_m. We conjecture that an increase in voltage or temperature can increase the dissociation rate of the polaron pairs and, accordingly, decrease the extrinsic low-field linewidth B_m. This is in agreement with our experimental

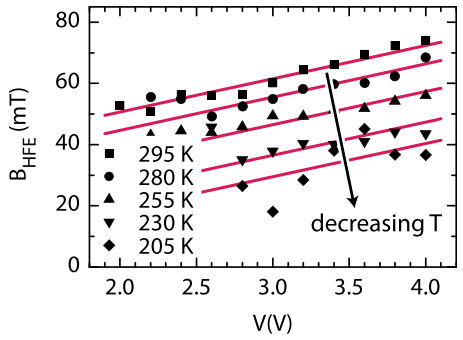

FIG. 7. Extracted high-field effect parameter as a function of voltage for different temperatures. The linewidth of the high-field effect B_{HFE} shows an increase in linewidth with increasing voltage and temperature.

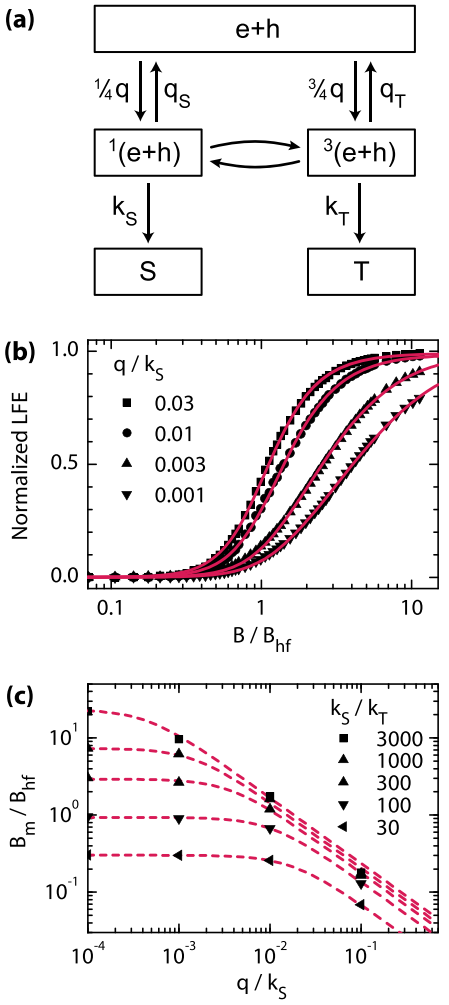

FIG. 8. Simulating the magnetic field effects linewidths. (a) Simulations for the LFE. (b) Normalized LFE as a function of the normalized magnetic field. (c) Additional broadening extracted from the simulations for the LFE. Dashed lines provide a guide to the eye.

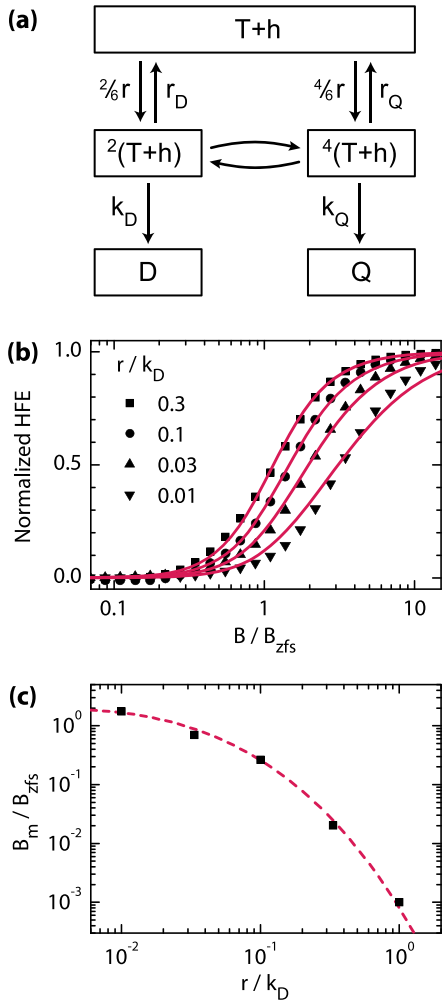

FIG. 9. Simulating the magnetic field effects linewidths. (a) Simulations for the high-field effect (HFE). (b) Normalized HFE as a function of the normalized magnetic field. (c) Additional broadening extracted from the simulations for the HFE. Dashed lines provide a guide to the eye.

results. Furthermore, the simulations show that this effect is more pronounced for a greater singlet to triplet recombination ratio. In passing, we note that the simulations do not take device physics into account, which could also cause additional broadening.

Finally, we have calculated the HFE for triplet–polaron interactions as a function of the magnetic field for different triplet–polaron dissociation (r_D) and reaction rates (k_D). The resulting lineshapes are shown in Fig. 9(b). The HFE lineshape shows a similar lineshape as the LFE, but, as mentioned before, on a different field scale (B_{ZFS} instead of B_{hf}). From the calculations, we can conclude that an increase in reaction rate, while keeping the other rates in the system constant, causes additional broadening of the MC(B)-curves even though B_{ZFS} is kept constant. We have also analyzed the HFE lineshape using our empirical function. In this case, the intrinsic linewidth, which is governed by B_{ZFS} instead of B_{hf}, is also fixed so that the only free fitting parameter is the extrinsic broadening parameter B_m. The result is shown in Fig. 9(c). We conjecture that an increase in voltage or temperature could lead to an increase in reaction rate, explaining the experimental results in Fig. 7. Please note that, to the best of our knowledge, these calculations are the first to show the influence of the different triplet–polaron reaction rates on the HFE lineshape.

IV. CONCLUSION

In conclusion, we have investigated the magnetic field effect on the current for a wide range of temperatures and voltages. Using a full quantitative analysis of the lineshapes, we are able to extract all linewidth parameters (both the linewidths and amplitudes) and explain their voltage and temperature dependence accordingly. We attribute the MFEs to the recently proposed trion mechanism.[23] We analyzed the MC(V)-curves using the analytical model as proposed by Cox *et al.* and confirmed the physical validity of the fitting parameters. The linewidths of the low-field effects have been analyzed and we show that the hyperfine field strength B_{hf} is almost identical for all measurements, whereas B_m and r do show a remarkable voltage and temperature dependence. Finally, the high-field effect linewidth B_{HFE} also show a surprising voltage and temperature dependence. Preliminary results on microscopic simulations show a qualitative agreement to the experimental results. This opens up unprecedented routes towards a deeper fundamental understanding of the relevant triplet polaron reaction rates for OMAR.

ACKNOWLEDGMENTS

This work was supported by the Dutch Technology Foundation STW via the NWO VICI grant "Spin Engineering in Molecular Devices" (Project No. 06628) and NWO NANO Grant "Chasing the spin in organic spintronics" (Project No. 11424).

[1]J. Kalinowski, M. Cocchi, D. Virgili, P. Di Marco, and V. Fattori, Chem. Phys. Lett. **380**, 710 (2003).
[2]T. L. Francis, O. Mermer, G. Veeraraghavan, and M. Wohlgenannt, New J. Phys. **6**, 185 (2004).
[3]Ö. Mermer, G. Veeraraghavan, T. Francis, and M. Wohlgenannt, Solid State Commun. **134**, 631 (2005).
[4]F. L. Bloom, W. Wagemans, M. Kemerink, and B. Koopmans, Phys. Rev. Lett. **99**, 257201 (2007).
[5]F. L. Bloom, W. Wagemans, and B. Koopmans, J. Appl. Phys. **103**, 07F320 (2008).
[6]S. A. Bagnich, U. Niedermeier, C. Melzer, W. Sarfert, and H. von Seggern, J. Appl. Phys. **106**, 113702 (2009).
[7]S. Zhang, A. Drew, T. Kreouzis, and W. Gillin, Synth. Met. **161**, 628 (2011).
[8]B. Hu and Y. Wu, Nature Mater. **6**, 985 (2007).
[9]F. J. Wang, H. Bässler, and Z. Valy Vardeny, Phys. Rev. Lett. **101**, 236805 (2008).
[10]N. J. Rolfe, M. Heeney, P. B. Wyatt, A. J. Drew, T. Kreouzis, and W. P. Gillin, Phys. Rev. B **80**, 241201 (2009).
[11]W. Wagemans, P. Janssen, E. H. M. van der Heijden, M. Kemerink, and B. Koopmans, Appl. Phys. Lett. **97**, 123301 (2010).
[12]W. P. Gillin, S. Zhang, N. J. Rolfe, P. Desai, P. Shakya, A. J. Drew, and T. Kreouzis, Phys. Rev. B **82**, 195208 (2010).
[13]T. D. Nguyen, G. Hukic-Markosian, F. Wang, L. Wojcik, X.-G. Li, E. Ehrenfreund, and Z. V. Vardeny, Nature Mater. **9**, 345 (2010).
[14]W. Wagemans, A. J. Schellekens, M. Kemper, F. L. Bloom, P. A. Bobbert, and B. Koopmans, Phys. Rev. Lett. **106**, 196802 (2011).
[15]J. Rybicki, R. Lin, F. Wang, M. Wohlgenannt, C. He, T. Sanders, and Y. Suzuki, Phys. Rev. Lett. **109**, 076603 (2012).

[16]W. Baker, K. Ambal, D. Waters, R. Baarda, H. Morishita, K. van Schooten, D. McCamey, J. Lupton, and C. Boehme, Nat. Commun. **3**, 898 (2012).
[17]V. Prigodin, J. Bergeson, D. Lincoln, and A. Epstein, Synth. Met. **156**, 757 (2006).
[18]P. Desai, P. Shakya, T. Kreouzis, W. P. Gillin, N. A. Morley, and M. R. J. Gibbs, Phys. Rev. B **75**, 094423 (2007).
[19]P. A. Bobbert, T. D. Nguyen, F. W. A. van Oost, B. Koopmans, and M. Wohlgenannt, Phys. Rev. Lett. **99**, 216801 (2007).
[20]P. Janssen, M. Cox, M. Kemerink, M. Wienk, and B. Koopmans, Nat. Commun. **4**, 2286 (2013).
[21]W. Wagemans, P. Janssen, A. J. Schellekens, F. L. Bloom, P. A. Bobbert, and B. Koopmans, SPIN **01**, 93 (2011).
[22]J. Y. Song, N. Stingelin, A. J. Drew, T. Kreouzis, and W. P. Gillin, Phys. Rev. B **82**, 085205 (2010).
[23]M. Cox, P. Janssen, F. Zhu, and B. Koopmans, Phys. Rev. B **88**, 035202 (2013).
[24]P. Blom and M. Vissenberg, Mater. Sci. Eng., R **27**, 53 (2000).
[25]M. Cox, P. Janssen, S. H. W. Wouters, E. H. M. van der Heijden, M. Kemerink, and B. Koopmans, Synth. Met. **173**, 10 (2013).
[26]D. Hertel and K. Meerholz, J. Phys. Chem. B **111**, 12075 (2007).
[27]M. Kuik, L. J. A. Koster, G. A. H. Wetzelaer, and P. W. M. Blom, Phys. Rev. Lett. **107**, 256805 (2011).
[28]A. Kadashchuk, V. I. Arkhipov, C.-H. Kim, J. Shinar, D.-W. Lee, Y.-R. Hong, J.-I. Jin, P. Heremans, and H. Bässler, Phys. Rev. B **76**, 235205 (2007).
[29]G. G. Malliaras, J. R. Salem, P. J. Brock, and J. C. Scott, J. Appl. Phys. **84**, 1583 (1998).
[30]M. Kemerink, J. Kramer, and H. Gommans, Appl. Phys. Lett. **88**, 192108 (2006).
[31]A. J. Schellekens, W. Wagemans, S. P. Kersten, P. A. Bobbert, and B. Koopmans, Phys. Rev. B **84**, 075204 (2011).
[32]P. A. Bobbert, W. Wagemans, F. W. A. van Oost, B. Koopmans, and M. Wohlgenannt, Phys. Rev. Lett. **102**, 156604 (2009).